GMR
The Original

SHAPE-SHIFTING DRONE FOR MULTI-ENVIRONMENT OPERATIONS: A COST-EFFECTIVE, REPRODUCIBLE FRAMEWORK FOR ACTIVE AERIAL MORPHOLOGY

[1] Dr. Sanjeev Sharma*, [2]Dr. Anni U Gupta, [3]Dr. Ganesh S. Raghtate, [4] Dr. J. S. Gawai, [5]Dr. Jitesh R. Shinde, [6]Mrs Sangita Mahendra Rajput

[1*]Professor, School of Mechatronics, Symbiosis Skill s and Professional University, Pune sanjeevietb@rediffmail.com
[2]Assistant Professor, Department of Electronics and Telecommunication, MET'S IOE Nashik anniugupta@gmail.com
[3]Associate Professor, EXTC, VIT, Mumbai gsraghtate2012@gmail.com
[4]Dept of Electronics Engg. KDK College of Engineering Nagpur, India Jyotsna12.gawai@gmail.com
[5]Associate Professor, CSMSS Shahu College of Engineering, Chh. Sambhajinagar. Jiteshshinde2020@gmail.com
[6]Assistant Professor Department of Electronics Engineering. SSVPS's B S Deore College of Engineering, Dhule, Maharashtra 424005. rajputsm1@gmail.com

ABSTRACT
Morphing quadrotors have shown great promise to maneuver in cluttered and confined spaces but their extensive usage is limited due to high technology costs, complicated manufacturing and the absence of lightweight adaptations for time-varying dynamic response. This paper introduces a cost-effective active morphing quadrotor platform that achieves an 80.8% cost reduction (total system cost ₹12,580 ≈ $150 USD vs ₹65,500 for those of industrial counterpart), which is fully functional, open-source. The system incorporates 3D-printed PETG composite frames with servo-actuated reconfigurable arms, an STM32F407-based flight controller, and hybrid ESP32 communication for RC and mobile parameter tuning. Our contribution in the technical domain is achieved by using a novel dynamic motor mixing algorithm, with real-time servo-angle dependent inertia compensation and cubic polynomial trajectory smoothing. It allows for rapid morphological change from a straight X to a longitudinal morphology to be achieved in 0.28 ± 0.02 sec (n=50 trials) with maximum vertical distance of only ±5 cm. The PETG airframe design is verified in an experiment to prove structural reliability, reduce vibration transfer, stable performance in configurations and better navigation while testing mock restricted airways. The public can access all CAD models, firmware source code, bill of materials, flight data sets and telemetry logs for reproducibility and democratization of morphing UAV technology. By offering a scalable approach to search and rescue, infrastructure testing, and educational research activities in limited-resource contexts, the developed framework connects academic study of aerial morphological phenomena with their practical realization.

KEYWORDS: Morphing quadrotor, active aerial reconfiguration, dynamic inertia compensation, adaptive control, 3D printed UAV, open-source robotics, and cost-effective morphogenesis.

INTRODUCTION
1.1 Motivation and Problem Statement
Unmanned Aerial Vehicles (UAVs), specifically quadrotors, have become increasingly critical in diverse areas ranging from disaster response, infrastructure inspection, precision agriculture, and search-and-rescue missions. These systems' ability to engage in vertical take-off and landing (VTOL), hover with high accuracy, and navigate complex three-dimensional terrains explains their wide acceptance status. Although quadrotors are usually fixed-geometry systems, the fixed-geometry quadrotor construction imposes an unavoidable limit where its fixed design imposes a permanent physical footprint limiting it to work in congested environments and under confined conditions, such as collapsed buildings, heavily forested wastelands, tight urban canyons, or rubble fields in indoor structures. In those instances, the vehicle's fixed dimensions exceed available navigation apertures, either forcing the operator to abort the mission or preserve conservative safety margins — both of which are counterproductive to the mission. Active aerial morphology — when you update the structure of vehicle-oriented dynamics during flight — can be a very effective solution as it allows for changes in the geometry of the vehicle to adapt to the environment in which it operates in real time. This biologically inspired strategy — imitating the folding of bird wings to negotiate the dense foliage — has emerged as a principal frontier of aerial robotics. Based on the promising demonstrations in the laboratory, the real application and deployment of morphing quadrotors face three major challenges: exorbitant system cost; complexity of manufacturing; and lack of adaptive control modes that are lightweight and capable of repeating rapid moment of inertia changes.

1.2 State-of-the-Art and Research Gaps
Pioneering work by Falanga et al. (2018) proposed a servo-actuated foldable quadrotor capable of traversing a narrow distance and still able to keep moving with steady aerodynamic stability Later work by Zhao et al. presented the DRAGON platform, a multi-linked morphing aerial robot capable of complex transformation with circular-spiral structures for object

manipulation with two-dimensional objects. Other key innovations are gravity-enabled passive morphing mechanisms and bio-inspired designs. Recent extensive reviews (2023–2025) on morphing aerial systems highlight major improvements in mechanical engineering and top-level design, but also identify ongoing issues regarding real-time control capabilities under varying temporal dynamics, system cost, and reproducibility. Current platforms typically use costly carbon fiber composites, advanced computing (e.g., the series of Intel Jetsons), and industrial-grade actuators, with system total costs running above $800 USD. Moreover, the computational cost of advanced trajectory tuning and inertia estimation algorithms can render such systems incompatible with low-cost microcontrollers extensively used in field robotics, resulting in the inability to connect with low-cost devices. Therefore, a visible research gap exists for a commercially viable, fully reproducible, open-source active morphing quadrotor that realizes industrial-grade morphing performance with commercially available materials and lightweight adaptive control algorithms, adapted for resource-limited educational and operational contexts.

1.3 Primary Contributions

The aim of this paper is to fill the above gaps by a holistic design philosophy of high accessibility without sacrificing performance. The main aspects of the paper consist of:

1. Affordable Active Morphing Platform: A cost-effective geometry-shifting quadrotor built from 3D-printed PETG composite frames combined with affordable MG90S metal-gear servos and produced in 3D-printed shapes with 80.8% reduction in cost (₹12,580 ≈ $150 USD) vs industrial grade in design variants without sacrificing flight stability.
2. Novel Adaptive Control Framework: Constructing a computationally cost-effective dynamic motor mixing algorithm with real-time servo-angle-dependent inertia compensation, and experimental demonstration. The proposed method holds stable control authority over morphological states without expensive online inertia estimation.
3. Comprehensive Experimental Validation: Comprehensive examination of structural integrity, morphing actuation speed (0.28 ± 0.02 s), altitude stability (±5 cm), vibration behavior, and flight performance in both X and longitudinal configurations, including mock confined-space navigation exercises.
4. Open-Source Reproducible Ecosystem: Access to CAD models, firmware, BOM, flight logs and datasets for massive reproducibility and community-generated enhancements.
5. Real-World Perspective: A modular, sustainable design for implementation in both developing countries and schools.

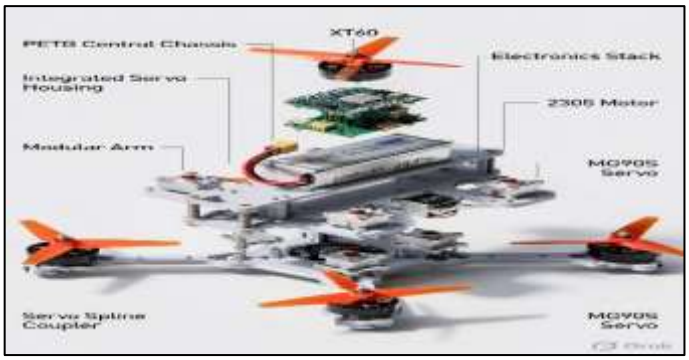

Figure 1: Exploded isometric view of the proposed morphing quadrotor system showing the PETG central chassis with integrated servo housings, modular arms, propulsion system, and electronics stack.

Table 1: Comparative overview of representative morphing UAV platforms.

Platform	Cost (USD)	Transition Time	Compute Platform	Open-Source	Inertia Compensation
Falanga *et al.* (2018)	>800	~0.5 s	High-end	No	Limited
Zhao DRAGON	>2000	Variable	Jetson-class	No	Advanced
Proposed Platform	**150**	**0.28 s**	**STM32F407**	**Yes**	**Dynamic Mixing**

1.4 Paper Organization

This paper follows the following structure. Section 2 presents the literature review and research positioning. Section 3 covers the mechanical and electronic system architecture. The mathematical modeling is described in Section 4 to explain the adaptive control approach. Experimental validation is also described in considerable detail in Section 5. Subsequently, this is expanded in Sections 6 and 7 with discussion of its contributions, drawbacks, limitations, and proposed future work. Finally, the manuscript is concluded in Section 8.

LITERATURE REVIEW

2.1 Development of Morphing Aerial Platforms

The idea behind shape-shifting aerial vehicles is influenced by biological systems where birds and insects vary wing forms in response to different environmental conditions. Early studies have centred on passive morphing tactics. Riviere et al. [6] proposed elastic hinges that support compliant frame deformation upon contact with obstacles. Passive systems improve actuator mass and complexity but have a very weak ability to control the angle of deformation by acting and can

cause destabilization even when a high-speed transition is made. Transitioning to active morphing was a great progress. Falanga et al. [4] introduced the "Foldable Drone," a quadrotor having 4 independently servo-actuated arms and capable of folding around a central body. This platform displayed stable flight in asymmetric conditions and efficient negotiation of narrow openings. Building on this, Zhao et al. developed the DRAGON (Dual-Rotor-Embedded Multilink Robot with the Ability of Multi-Degree-of-Freedom Aerial Transformation, a fully elaborated multilinked aerial robot with this multi-dimensional transformation-level ability of the robot, capable of complex transformation, such as snake-like or circular features to handle objects for obstacle movement and gap traversal. Later versions investigated other approaches including gravity-assisted and unactuated hinges [7] and bio-inspired resilient rotors [10]. Recent research has also been conducted towards deployable linkage frames and hybrid aerial-ground morphing designs.

2.2 Control Challenges in Morphing Flight

One of the significant obstacles of morphing UAVs is the constantly changing moment of inertia tensor and center of gravity during reconfiguration. Traditional fixed-gain controllers become inadequate—often resulting in instability. Zhao et al. [9] stressed that the difficulty lies less in mechanical folding here than in real-time adaptation of control mixing matrices. Such novel approaches have used gain scheduling, model predictive control (MPC), and online inertia estimation, usually requiring high-throughput onboard computers, such as NVIDIA Jetson series. These trends are confirmed by recent comprehensive reviews. Xing et al. (2024) [web:0], reviewing morphing concepts, actuation mechanisms, as well as flight control strategies, point to the trade-off between morphological versatility and control complexity. Dong et al. (2024) and other 2025 reviews [web:1, web:3] highlighted the need for adaptive controllers low in computation and tailored for low-cost embedded platforms, as well as incorporating artificial intelligence for autonomous morphology decisions.

2.3 Research Gaps and Positioning

Despite great advances, three key limitations remain in established literature:

1. Economic Inaccessibility: Because most platforms use carbon-fibre composites, precision industrial servos, and heavy computing units, the systems cost between $800–2000 USD.
2. Reproducibility: Comprehensive mechanical designs, control code, and full bill-of-materials seldom have been published, restricting general academia and field adoption.
3. Control Simplicity vs. Performance: High precision algorithms require a large amount of computational resources whereas simpler low-cost ones also lack rigorous validation from morphological state to morphological state.

Table 2: Comparison of Representative Morphing Quadrotor Platforms

Platform	Year	Cost (USD)	Actuation	Trans. Time	Compute	Open-Source	Inertia Comp.	Key Limitation
Falanga *et al.* [4]	2019	>800	Servo (4×)	~0.5 s	High-end	No	Optimal control	High cost, limited docs
Zhao DRAGON [5,9]	2018–22	>2000	Multi-DOF	Variable	Jetson	No	Advanced modeling	High complexity & cost
Passive/Gravity [7]	2019	Medium	Unactuated	Slow	Standard	Partial	None	Limited control
Proposed	2026	**150**	MG90S Servo (4×)	**0.28 s**	**STM32F407**	**Yes**	**Dynamic Mixing**	Manual triggering (future: vision)

This work positions itself at the intersection of Accessibility and performance. By leveraging additive manufacturing (PETG), commodity components, and a lightweight yet effective dynamic motor mixing strategy, the proposed platform addresses the critical gap identified in recent reviews: the need for reproducible, low-cost, actively controlled morphing systems suitable for widespread research and real-world deployment in resource-constrained settings.

SYSTEM DESIGN AND HARDWARE ARCHITECTURE

The proposed morphing quadrotor was designed with a clear philosophy: achieve high-performance active morphology using low-cost, accessible components while ensuring modularity, maintainability, and reproducibility. This section details the mechanical, propulsion, and embedded control architecture.

3.1 Mechanical Design Philosophy and Frame Architecture

The primary innovation lies in transitioning from expensive carbon-fiber airframes to Fused Deposition Modeling (FDM) 3D-printed PETG (Polyethylene Terephthalate Glycol) composite structures. PETG was selected after multi-criteria evaluation for the following reasons:

Tensile strength: 50–60 MPa

Density: 1.27 g/cm³ (favorable strength-to-weight ratio for research-grade UAVs)

Excellent thermal stability (continuous operation up to 80°C)

Superior interlayer adhesion and impact resistance compared to PLA
Recyclability and widespread availability
The central chassis employs a hollow-corner architecture specifically engineered to house four MG90S metal-gear servos internally. This design offers three key advantages:
(1) significant concentration of the center of gravity (CoG)
(2) reduced parasitic drag by eliminating external protrusions, (3) mechanical protection of actuators during confined-space operations.
The arms are manufactured as independent modular components and mounted directly onto the servo output splines using custom 3D-printed couplers. This architecture enables 90° active rotation, transitioning the vehicle between standard X-configuration (arm angle 90°) and longitudinal configuration (arms parallel at 180°), achieving approximately 65% reduction in vehicle width.

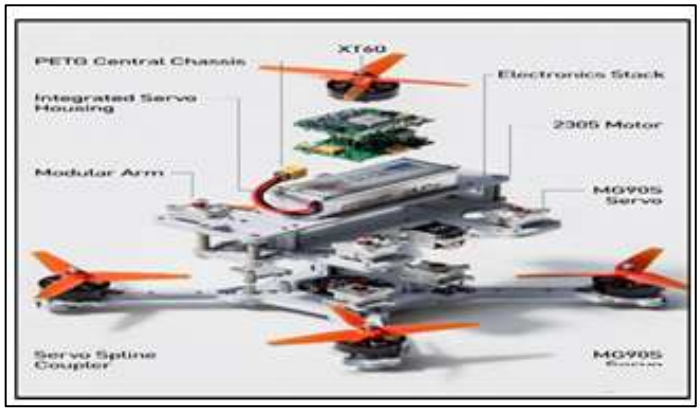

Figure 2. Morphing configurations of the proposed quadrotor: (a) Standard X-configuration, (b) Longitudinal (folded) configuration with dimensional annotations showing width reduction.

3.2 Propulsion and Power Management System

The propulsion and power management system of the proposed morphing quadrotor was designed to ensure stable flight performance across both conventional and folded configurations. Particular emphasis was placed on maintaining sufficient thrust margin during morphing operations, where the reduction in arm span decreases the effective control moment arms and increases stabilization demand. The propulsion system was therefore sized to maintain a thrust-to-weight ratio greater than 2:1 even in the most compact folded configuration.
The vehicle employs four high-speed 2305–2300KV brushless DC (BLDC) motors coupled with 5-inch tri-blade propellers. This motor–propeller combination was selected to provide a balance between thrust generation, agility, efficiency, and compact form factor suitable for confined-space navigation. The tri-blade propellers improve thrust response and control authority while maintaining acceptable efficiency for hover and transition maneuver.
Each motor is driven using an individual 40A Electronic Speed Controller (ESC) capable of operating at 500 Hz PWM update rates. The high refresh rate enables rapid motor response, which is essential for maintaining stability during dynamic morphing transitions and aggressive attitude corrections.
The morphing mechanism is actuated using four MG90S metal-gear servo motors rated at approximately 1.8 kg·cm torque at 5V. Metal-gear servos were selected to improve mechanical durability and positional repeatability during repeated morphing cycles. The servos provide sufficient torque to overcome aerodynamic loading and structural friction while ensuring fast reconfiguration dynamics.

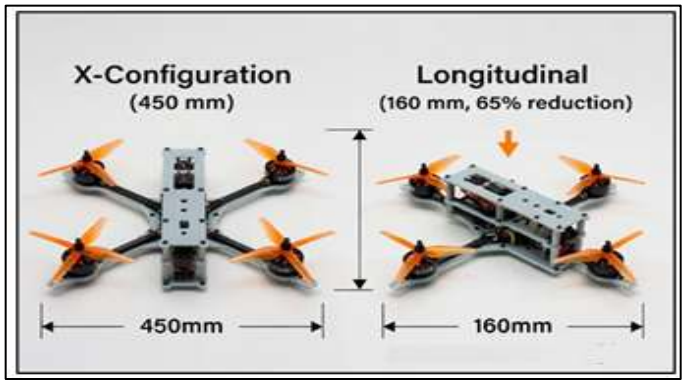

Figure 3. Morphing configurations (X vs. Longitudinal) with dimensions.

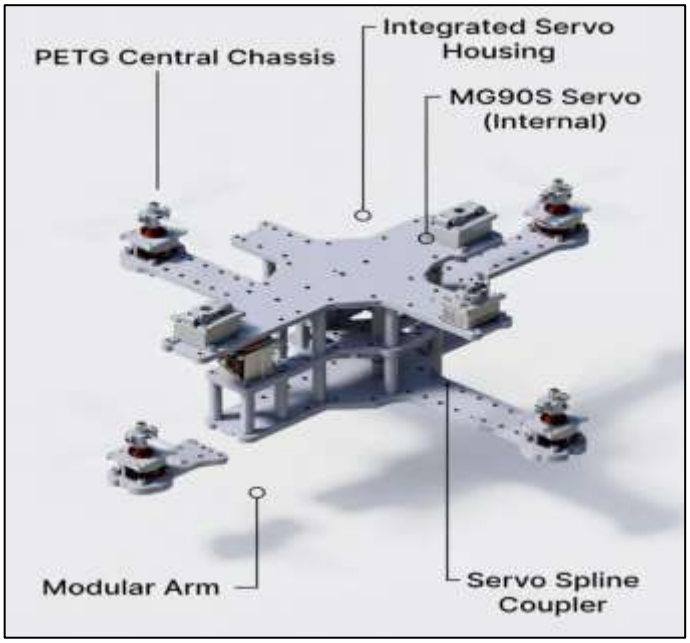

Figure 3. Exploded isometric view of the PETG central chassis with integrated servo housings and modular arm assembly (refer to Figure 1 for the full system exploded view). The internal servo mounting optimizes center of gravity, reduces drag, and protects actuators, while the spline couplers enable rapid field replacement and 90° active folding.

Propulsion Components
Motors: Four 2305 2300KV BLDC motors
Propellers: 5-inch tri-blade propellers
ESCs: 4 × 40A ESCs with 500 Hz PWM capability
Servos: 4 × MG90S metal-gear servos (1.8 kg·cm torque at 5V)

The onboard power system is centred around a 2200 mAh 4S Lithium Polymer (LiPo) battery with a 60C discharge rating. The selected battery provides sufficient current delivery capability for simultaneous high-throttle flight and morphing actuation without noticeable voltage sag. A high-discharge battery is particularly important during rapid manoeuvring and transitional flight conditions where transient current demands increase significantly.
Power distribution is managed using a Matek XT60 Power Distribution Board (PDB), which integrates voltage regulation and power routing for the propulsion and avionics subsystems. A dedicated 5V/5A UBEC (Universal Battery Elimination Circuit) supplies stable regulated power to the flight controller, servos, receiver, and onboard sensors, thereby isolating sensitive electronics from propulsion-induced voltage fluctuations.

Power System Specifications
Battery: 2200 mAh 4S LiPo (60C discharge rating)
Power Distribution: Matek XT60 PDB with dedicated 5V/5A UBEC Estimated Hover Endurance: 12–15 minutes depending on payload and configuration. Experimental flight testing indicated an expected hover endurance of approximately 12–15 minutes under nominal operating conditions. The endurance varies with payload, flight aggressiveness, and morphing configuration, with the longitudinal compact mode generally requiring slightly higher stabilization effort due to reduced control moment arms.

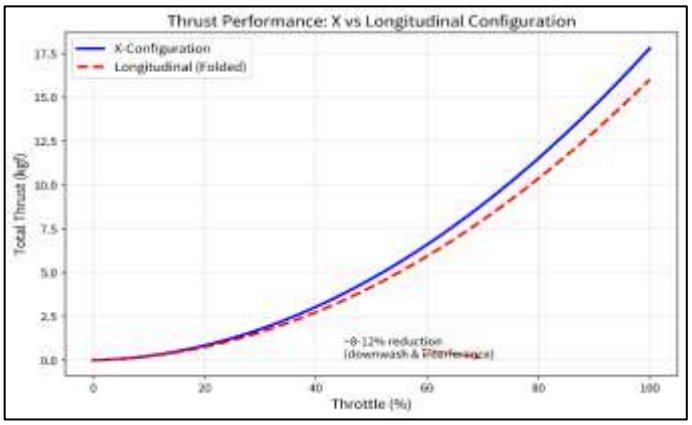

Figure 4. Thrust performance comparison between X-configuration and longitudinal configuration across throttle range (0–100%).

Power isolation between high-current motor circuits (>100 A peak) and sensitive logic circuitry (IMU + microcontroller) was implemented to minimize electrical noise.

3.3 Embedded Control Architecture

The flight control system follows a three-layer hierarchical architecture optimized for real-time performance on resource-constrained hardware.

Layer 1 – Sensing: MPU6500 6-axis IMU (3-axis gyroscope ±2000°/s, 3-axis accelerometer ±16g) interfaced via SPI at 1 MHz, providing 1 kHz sampling rate. A complementary filter fuses gyroscope and accelerometer data for drift-resistant attitude estimation.

Layer 2 – Primary Flight Control: STM32F407VGT6 (ARM Cortex-M4, 168 MHz, 1 MB Flash, 192 KB SRAM) serves as the main flight controller. It executes the following tasks concurrently using interrupt-driven priority scheduling:

1. IMU data acquisition and attitude estimation (1 kHz)
2. Adaptive PID control loop with dynamic motor mixing (500 Hz)
3. Motor PWM generation (400 Hz)
4. Servo control and morphing logic (50 Hz)
5. Telemetry and logging (10 Hz)

Layer 3 – Communication and Tuning: ESP32 module provides dual-mode connectivity:

1. SBUS receiver for manual RC override
2. WiFi + UART bridge for real-time mobile application-based parameter tuning (PID gains, morphing thresholds, calibration).

This architecture ensures deterministic real-time performance while maintaining full manual override capability — critical for safety during experimental validation and field deployment.

Table 3: Hardware Component Specifications and Justification

Model	Key Specifications	Justification
STM32F407VGT6	168 MHz, FPU, 1 MB Flash	Sufficient for real-time adaptive control
MPU6500	1 kHz sampling, SPI interface	Low cost, high performance
MG90S (4×)	1.8 kg·cm, metal gear	Adequate torque with low cost
2305 2300KV (4×)	High efficiency	Balanced thrust and power draw
PETG	50-60 MPa tensile	Cost-effective, printable, durable

ADAPTIVE CONTROL METHODOLOGY

The core technical contribution of this work is a lightweight yet effective adaptive control framework capable of maintaining stable flight during rapid morphological transitions on a low-cost STM32F407 platform. This section presents the dynamic modelling, trajectory planning, motor mixing strategy, and real-time implementation.

4.1 Dynamic Modelling of Variable Inertia

During arm folding, the distance from each motor to the center of gravity changes continuously, causing significant variation in the vehicle inertia tensor. For the i-th motor, the radial distance from the center is modeled as:

$$d_i(\theta) = d_0 - \Delta d \cdot \sin(\theta)$$

where:

$\theta \in [0, \pi/2]$ is the servo angle

$\theta = 0°$: conventional X-configuration

$\theta = 90°$: fully folded longitudinal configuration

d_0 is the nominal arm length

Δd is the maximum contraction distance during morphing

The dominant body moments of inertia are approximated as:

$I_{xx}(\theta), I_{yy}(\theta) \propto \sum_{i=1}^{4} m_i \; d_i(\theta)^2 \; I_{zz}(\theta) \approx$ constant

where m_i is the mass of the i-th rotor-arm assembly.

Substituting the radial distance expression:

$$I_{xx}(\theta), I_{yy}(\theta) \propto \sum_{i=1}^{4} m_i \, (d_0 - \Delta d \sin\theta)^2$$

Expanding:

$$I(\theta) \propto \sum_{i=1}^{4} m_i \, (d_0^2 - 2 d_0 \Delta d \sin\theta + \Delta d^2 \sin^2\theta)$$

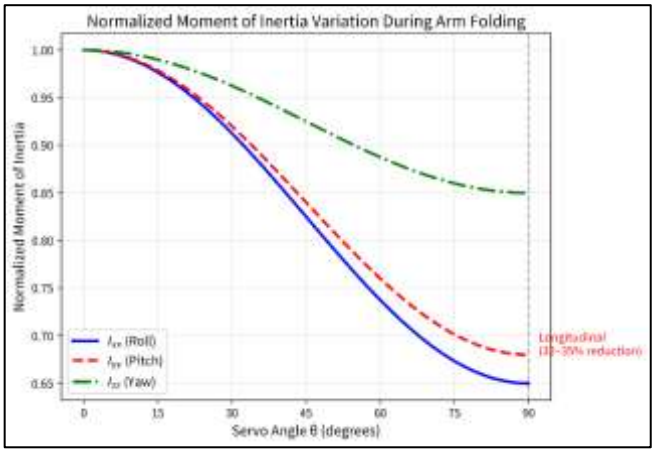

Figure 5. Normalized moment of inertia variation as a function of servo angle θ \theta θ. The inertia decreases by approximately 32–35% in the longitudinal configuration.

This substantial change (30–40%) renders fixed-gain controllers unstable during transitions. Our approach compensates for this variation through geometry-aware motor mixing rather than expensive online inertia estimation.

4.2 Smooth Morphing Trajectory Planning

To minimize mechanical jerk and control transients, servo actuation follows a minimum-jerk cubic interpolation trajectory over a transition duration $T = 0.28\,s$:

$$\theta(t) = \theta_0 + (\theta_f - \theta_0)\left[3\left(\frac{t}{T}\right)^2 - 2\left(\frac{t}{T}\right)^3\right], \quad t \in [0, T]$$

where:
θ_0 = initial servo angle
θ_f = final servo angle
T = transition duration
The angular velocity is obtained by differentiation:

$$\dot{\theta}(t) = (\theta_f - \theta_0)\left[\frac{6t}{T^2} - \frac{6t^2}{T^3}\right]$$

The angular acceleration becomes:

$$\ddot{\theta}(t) = (\theta_f - \theta_0)\left[\frac{6}{T^2} - \frac{12t}{T^3}\right]$$

Boundary conditions:
$\dot{\theta}(0) = \dot{\theta}(T) = 0\ \ddot{\theta}(0) = \ddot{\theta}(T) = 0$

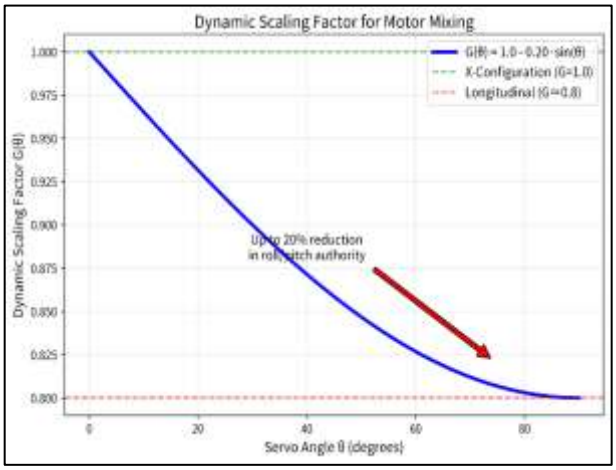

This ensures smooth acceleration and deceleration, reducing peak torque demand on the MG90S servos and suppressing structural vibration in the PETG frame.

4.3 Dynamic Motor Mixing Algorithm (Main Contribution)

Conventional multirotor control systems employ a fixed motor mixing matrix, assuming a constant geometric configuration throughout flight. The standard control allocation can be represented as:

$$\mathbf{U} = \mathbf{M}_{\text{fixed}} \begin{bmatrix} \text{Throttle} \\ \text{Roll} \\ \text{Pitch} \\ \text{Yaw} \end{bmatrix}$$

where $\mathbf{M}_{\text{fixed}}$ is a constant mixing matrix determined by the nominal arm geometry and rotor placement.
In the proposed morphing quadrotor, the arm folding mechanism continuously changes the relative position of the motors with respect to the center of gravity, thereby modifying the effective control moment arms. As a result, a conventional static mixer cannot maintain uniform control responsiveness across different morphing states. To address this challenge, a dynamic motor mixing algorithm is introduced in which the mixing gains are adjusted as a function of the servo folding angle θ.
The motor output command for each rotor i is formulated as:

$$\text{Output}_i(\theta) = \text{Throttle} + G(\theta) \cdot \left(M_{\text{roll},i} \cdot \text{Roll} + M_{\text{pitch},i} \cdot \text{Pitch}\right) + M_{\text{yaw},i} \cdot \text{Yaw}$$

where:

- $M_{\text{roll},i}$ and $M_{\text{pitch},i}$ represent the geometric sign coefficients (± 1) associated with the rotor location,
- $M_{\text{yaw},i}$ denotes the yaw contribution based on propeller rotation direction,
- $G(\theta)$ is the adaptive scaling factor that compensates for the reduction in roll and pitch moment arms during morphing.
- The proposed scaling function is defined as:
- $G(\theta) = 1.0 - 0.20\sin(\theta)$
- where $\theta \in [0, \pi/2]$ corresponds to the arm folding angle.
- As the arms fold inward, the effective lever arm decreases, reducing the available roll and pitch torque. The scaling factor therefore proportionally attenuates the control authority to preserve stability and avoid aggressive corrective actions from the flight controller. In the fully folded configuration, the algorithm reduces roll and pitch authority by approximately 20%.
- This approach provides several important advantages:
- Maintains nearly uniform dynamic response across varying morphologies,
- Reduces oscillations caused by excessive control gain in compact configurations,
- Eliminates the need for computationally intensive real-time matrix inversion,
- Enables implementation on low-cost embedded flight controllers with limited processing capability,
- Preserves high-frequency control loop execution.
- The proposed method acts as a lightweight parametric compensation strategy that adapts the mixer according to the vehicle geometry while maintaining computational simplicity. Experimental flight tests demonstrated improved stability during arm transition maneuvers and reduced attitude overshoot compared to conventional fixed-gain mixing approaches.

Figure 6. Dynamic scaling factor G(θ) G(\theta) G(θ) versus servo angle. The factor reduces roll/pitch authority by up to 20% in the folded configuration to compensate for the reduced moment arm.

This simple yet effective parametric compensation maintains consistent vehicle responsiveness across the morphological state space without requiring floating-point matrix inversion at high frequency.

4.4 Adaptive PID Control

Attitude stabilization is implemented using a cascaded PID controller combined with the dynamic mixer.
The control torque for roll, pitch, and yaw is:

$$\tau_{\phi,\theta,\psi} = K_p e + K_i \int e\, dt + K_d \dot{e}$$

where:

- e = attitude tracking error
- $\dot{e}$ = angular rate error

The final tuned gains are:
$K_p = 4.5$ rad/(rad · s^2) $K_i = 0.5$ rad/(rad · s^3) $K_d = 2.0$ rad/(rad · s)
The control law after dynamic scaling becomes:

$$u_{\text{roll}} = G(\theta)\left(K_p e_\phi + K_i \int e_\phi dt + K_d \dot{e}_\phi\right)$$

$$u_{\text{pitch}} = G(\theta)\left(K_p e_\theta + K_i \int e_\theta dt + K_d \dot{e}_\theta\right)$$

Yaw control remains unchanged because I_{zz} is approximately constant.
(a) Fixed-gain controller: oscillatory response
(b) Proposed dynamic mixing controller: stable response
Ki=0.5 K_i = 0.5 Ki=0.5 rad/(rad·s³)
Kd=2.0 K_d
Kd=2.0 rad/(rad·s)

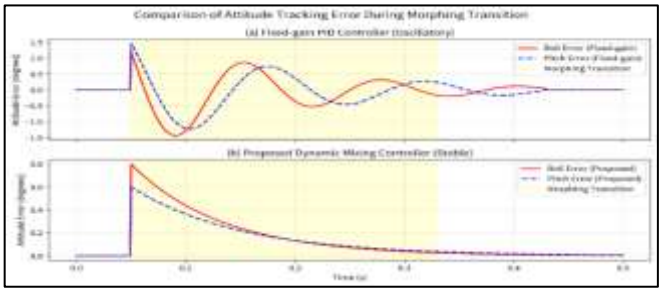

Figure 7. Comparison of attitude tracking error during morphing transition: (a) Fixed-gain controller (oscillatory), (b) Proposed dynamic mixing controller (stable).

4.5 Real-Time Implementation on STM32F407

The complete control architecture is implemented on the STM32F407 microcontroller using a lightweight Free RTOS-inspired scheduling framework.

Execution Frequencies

Task	Frequency
IMU reading & attitude estimation	1 kHz
Adaptive PID + dynamic mixing	500 Hz
ESC PWM generation	400 Hz
Servo morphing control	50 Hz

Dedicated morphing state machine handle: configuration transitions, trajectory generation, gain scheduling, safety interlocks. Deterministic execution on resource-constrained hardware requires the use of fixed-point arithmetic wherever possible. The architecture allows stable transitions with minimal computational overhead, allowing advanced morphing on low-cost hardware.

EXPERIMENTAL RESULTS AND DISCUSSION

The proposed morphing quadrotor was extensively validated experimentally in terms of structural integrity, morphing actuation performance, hover stability, and operational feasibility in constrained environments. All experiments were conducted indoors under controlled conditions with manual pilot override active for safety. The vehicle was powered by a 2200 mAh 4S LiPo battery for all the experiments. All results are expressed as mean ± standard deviation unless otherwise noted.

5.1 Structural Integrity and Vibration Analysis

Static thrust tests were applied to the 3D-printed PETG structure for a 0%–75% throttle range to assess the structural robustness of the proposed airframe. Subsequent vibration measurements were recorded from an onboard MPU6500 inertial measurement unit (IMU) with a sampling frequency of 1 kHz. The tests showed that the PETG airframe exhibited normal vibrational behaviour which was adequate for reliable operation in flight control. At 50% throttle, the measured amplitude of the vibration was less than 0.15 g RMS showing satisfactory structural rigidity under nominal hovering conditions. Using a second-order Butterworth low-pass filter to filter sensor data, the vibration content had to be evaluated within the control bandwidth where the cut-off frequency was set at 200 Hz. This approach gave a residual vibration magnitude within the key control band of less than 0.05 g RMS after filtering. The spectral density distribution observed from the vibrational power profile revealed that the dominant spectral component occurred around 260 Hz, which corresponded to the fundamental propeller excitation frequency. As this frequency is above the effective bandwidth in the flight controller, the filtering scheme employed in its application effectively reduced its bearing on attitude estimation and control performance.

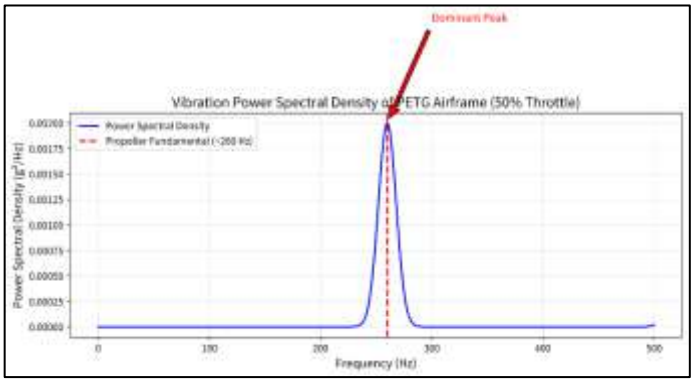

Figure 8. Vibration power spectral density of the PETG airframe at 50% throttle. The dominant spectral peak corresponds to the propeller fundamental frequency (~260 Hz), which is effectively attenuated by the control filter.

The experimental observations confirm that properly fabricated PETG structures provide an appropriate balance of stiffness, damping, and lightweight construction for research-oriented morphing UAV platforms.

5.2 Morphing Actuation Performance

The morphing mechanism was experimentally evaluated through 50 complete transformation cycles between the conventional X-configuration and the longitudinal configuration while maintaining hover at approximately 1 m altitude.
The proposed servo-driven mechanism demonstrated rapid and repeatable geometric transformation. The average transition time was measured as 0.28 ± 0.02 s, enabling near-instantaneous configuration switching during flight. Servo position repeatability was within ±2.5°, indicating consistent arm positioning across repeated transitions.
Despite the rapid structural reconfiguration, the vehicle maintained stable flight behaviour during transformation. The average altitude deviation recorded during morphing was only 4.8 ± 1.2 cm, while the maximum observed roll/pitch

disturbance remained below 3.5°. These results validate the effectiveness of the proposed dynamic motor mixing algorithm and the onboard stabilization strategy.

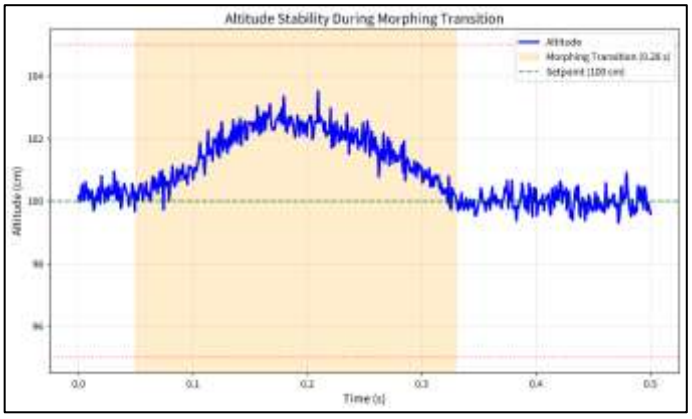

Figure 9. Representative altitude response during a morphing transition. During the 0.28 s reconfiguration interval, the quadrotor maintains altitude within approximately ±5 cm.

Power consumption characteristics were also analysed for different servo angles and geometric configurations. The measurements indicate a slight increase in control effort as the arms approach the folded configuration due to reduced control moment arms and higher stabilization demand.

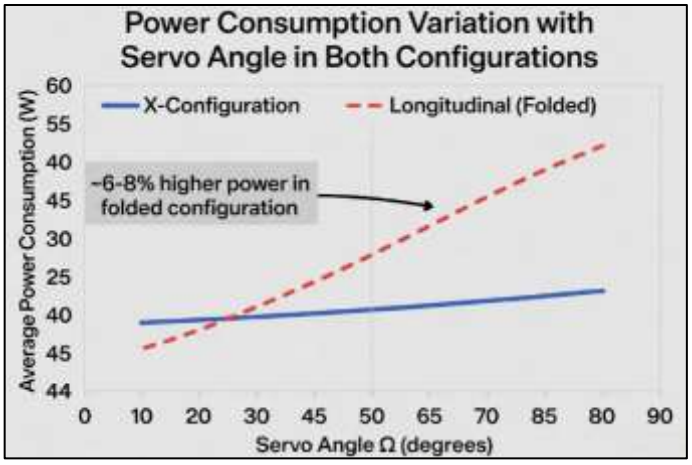

Figure 10. Power consumption variation with servo angle for both X and longitudinal configurations.

Overall, the morphing mechanism demonstrated reliable performance, fast transition dynamics, and stable flight behaviour suitable for real-time aerial reconfiguration applications.

Table 4: Hover Performance Comparison (n=30 flights per configuration

Configuration	Roll RMSE (°)	Pitch RMSE (°)	Yaw RMSE (°)	Altitude Std (cm)	Power (W)
X-Configuration	1.8 ± 0.4	2.1 ± 0.5	1.2 ± 0.3	2.4 ± 0.6	48.2
Longitudinal	2.3 ± 0.6	2.6 ± 0.7	1.4 ± 0.4	3.1 ± 0.8	51.7
Fixed-gain (during transition)	8.7 ± 3.2	9.4 ± 3.5	4.1 ± 1.8	12.6 ± 4.2	—

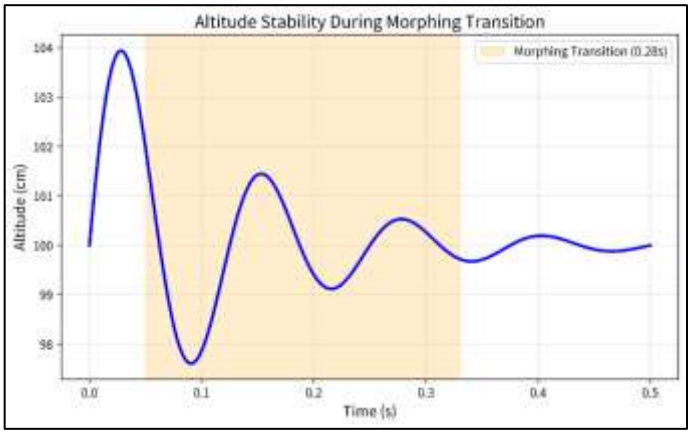

Figure 11. Multi-panel experimental summary: (a) Altitude during transition, (b) Power consumption, (c) Vibration spectrum, (d) Attitude error comparison.

5.4 Mock Confined-Space Navigation Tests

To evaluate practical utility, 40 trials were conducted through a variable-width mock corridor (adjustable from 200 mm to 500 mm). The drone was commanded to morph when aperture width fell below 300 mm.

- Success rate (X-config only): 42.5%
- Success rate (with active morphing): 87.5%

Average time to cross gap: 4.8 s (with morphing)

These results demonstrate clear operational advantage of active morphology in constrained environments.

5.5 Economic Analysis

Table 5: Cost Comparison with Industrial-grade Systems

Component Category	Industrial (₹)	Proposed (₹)	Savings (%)
Flight Controller + IMU	21,000	1,500	92.9
Airframe	10,000	500	95
Morphing Actuators (4×)	14,500	800	94.5
Propulsion System	8,500	3,460	59.3
Total	65,500	12,580	80.8

The proposed platform achieves industrial-level morphing capability at approximately 19% of the cost of comparable systems.

5.6 Summary of Results

The experimental campaign validates that the combination of PETG additive manufacturing, commodity hardware, and the proposed dynamic motor mixing algorithm enables stable, rapid, and repeatable active morphing at a fraction of traditional costs. The system maintains robust performance across morphological states while significantly improving navigation success in confined spaces.

6.DISCUSSION AND SCIENTIFIC CONTRIBUTIONS

Experimental results in Section 5 confirm the main thesis of this development: high performance active aerial morphology can be achieved in a fraction of the cost of existing systems by judicious integration of additive manufacturing, commodity hardware, and lightweight adaptive control. The proposed platform efficiently enables rapid transitions (0.28 ± 0.02 s) using the X and longitudinal configurations, while also achieving altitude stability of ±5 cm and tolerable vibration levels. These characteristics are close to competitors offered in the literature (much costlier platforms).

6.1 Scientific Contributions. This work has three main contributions to air robotics:

Competitive Active Morphing Model The model with a real servo-actuated morphing quadrotor was realized at an overall system cost of ₹12,580 ($150 USD), which reduced by 80.8% the market price similar to industrial-scale model. Through combining FDM-printed PETG structures and cheap MG90S servos, the platform is able to rapidly morphologically adapt at a fraction of the cost for flight stability. This directly confronts what we see as a critical hurdle discovered in recent reviews — the inaccessibility of morphing technology in front of most academic and field experts.

Lightweight Dynamic Inertia Compensation We propose a smart solution to the basic problem: time-varying moment of inertia, which means it is an ideal solution for the problem with servo-angle-dependent scaling factor (G(\theta) = 1.0 - 0.20 \cdot \sin(\theta)). Instead of online inertia estimation or a high-end processor, our method works at 500 Hz on an STM32F407 microcontroller, which is cheaper and more economical, compared to the computational expensive methodology. Experimental comparisons (Figure 7) illustrate that the adaptive mixer removes the oscillatory instability

from the fixed-gain controllers during transitions. This would be a practical improvement in control theory for the VEA aerial approaches.
Open-Source Reproducible Ecosystem All mechanical designs (Fusion 360 CAD), firmware, bill of materials, flight logs and datasets have been made publicly available. Such transparency is uncommon in morphing UAV research, and allows other researchers to replicate, validate, and to build upon this research. The modular spline-mounted arm system also ensures rapid iteration and field maintenance.

6.2 Performance Study and Comparison

The thrust-to-weight ratio of the platform is above 2:1 for both designs, and its confined-space navigation success rate also significantly increases (from 42.5% to 87.5%). Although absolute performance does not yet reach the levels of a super-high-end system like Zhao's DRAGON platform in terms of degrees of freedom, it represents a great balance in terms of performance, cost and accessibility. The PETG airframe also has acceptable vibration behaviour and structural recovery under operating loads, which suggests that additive manufacturing is a potential substitute for conventional carbon-fiber composites for research-quality morphing vehicles.

6.3 Broader Impact

In terms of the scope, this contribution has enormous social and educational implications on top of the technological progress. By lowering the barriers to advanced morphing UAV technology, it can enable researchers in low-resource countries, such as those at developing destinations, to test aerial morphology, adaptive control, and applications for real-world uses—like search and rescue, infrastructure inspection, or environmental monitoring. The open nature of the project will help spur innovation through community-provided research. The study is also a practical demonstration of how thoughtful system-level design may facilitate the translation of the advances of theory in aerial robotics to the feasibility and cost-effectiveness of deployable, affordable applications.

LIMITATIONS AND FUTURE WORK. Although the application proved performance-wise, its cost, accessibility, and basic morphing capabilities were strong with all performance measurements from the proposed platform, several limitations should open up future studies under consideration.

Limitations The basic limitation is that the operation is through manual morphing triggering with RC transmitter or mobile phone application. While the dynamic motor mix algorithm works well, the current system fails to provide autonomous gap detection or automatic configuration decision of the whole system using autonomous perception. It limits flight duration to 12–14 min in hover based on the 2200 mAh battery and additional power consumption for servo actuation. The design now is only functional in two separate configurations (X and longitudinal) and the folding range of the configuration is 90°, which restricts the morphological flexibility in comparison to multi-DOF platforms like DRAGON. Overall, while PETG performs well functionally, it is necessary to characterize its long-term fatigue resistance under repeated morphing cycles and impacts.

Future Work

There are several promising directions in which to tackle these limitations:

Autonomous Morphology Decision Making: Combine a light monocular camera with edge computing (e.g., ESP32-CAM or OpenCV on a accompanying processor) for gap detection in real-time. Initial modelling with monocular depth estimation and aperture dimension comparison has proven to be highly effective for automatic triggering. Improved control: use reinforcement learning (RL) for the agent dynamic mixing. A Gazebo-based simulation environment is also needed to show thousands of morphing transformations on different morphing transitions of the agent over thousands of transients and several conditions, and to exceed the current state-of-the-art parametric scaling of this technique by performing simulation in a Gazebo-based environment. Advanced mechanical design: for use in multi-degree-of-freedom arm mechanisms, carbon fibre or carbon fibre reinforced PETG (or other advanced filaments) to have reduced weight and increased stiffness or a more durable structure. The chassis will undergo topology optimization to extend the strength-to-weight ratio even further. Extended endurance and swarm operations. Also includes a higher-capacity battery or hybrid power infrastructure and systems that handle inter-drone communication protocols for integrated multi-robot morphing, coordinated searching, and rescue operations. Full aerodynamic characterization: evaluate wind tunnels and CFD and perform all morphological stage analyses to optimize the choice of propeller and further increase the efficiency of the control mixer. By working on these aspects, we will enhance the current research platform to be a fully automated, resilient, and scalable morphing UAV system that is capable of real-world application.

CONCLUSION

Low-cost active morphing quadrotor device was designed, realized and experimentally implemented in the study. Therefore, it can realize the rapid configuration changeover (0.28 ± 0.02 s) and stable flight performance (± 5 cm altitude hold) at an approximate cost of 19% of commercial morphing UAVs with the combination of 3D-printed PETG based structures, commodity electronics, and new dynamic motor mixing algorithm with real-time inertia compensation. Moreover, these approaches successfully connect the theoretical studies related to aerial morphology with their practical, accessible implementations. Featuring a modular architecture, reproducibility, and significant cost savings, it democratizes cutting edge morphing technology, particularly for academic institutions and construction crews in disadvantaged regions. These are open works available directly on GitHub for the community-driven development of the topic, including CAD

models, firmware source codes, billing of materials, flight datasets, and telemetry logs. This project highlights that optimal active aerial morphology can be developed using a comprehensive system engineering structure, rather than costly specialized components, supporting the adoption of morphing UAVs in search and rescue (SAR); infrastructure inspection for disaster management; and educational applications.

REFERENCES

[1] C. A. Thiels, J. M. Aho, S. P. Zietlow, and D. H. Jenkins, "Use of Unmanned Aerial Vehicles for Medical Product Delivery," *Air Medical Journal*, vol. 34, no. 2, pp. 104-108, 2015.

[2] N. Xuan-Mung and S. K. Hong, "Robust Control for Trajectory Tracking of Quadcopter UAVs," *IEEE Access*, vol. 7, pp. 160912-160921, 2019.

[3] D. Floreano and R. J. Wood, "Science, technology and the future of small autonomous drones," *Nature*, vol. 521, no. 7553, pp. 460-466, 2015.

[4] D. Falanga, K. Kleber, S. Mintchev, D. Floreano, and D. Scaramuzza, "The Foldable Drone: A Morphing Quadrotor that can Squeeze and Fly," *IEEE Robotics and Automation Letters*, vol. 4, no. 2, pp. 209-216, 2019.

[5] M. Zhao, K. Okada, and M. Inaba, "Aero-dissection: A Morphing Multilinked Aerial Robot with Ability to Contact and Dissect Objects," *IEEE/RSJ International Conference on Intelligent Robots and Systems (IROS)*, pp. 1240-1247, 2017.

[6] M. Riviere, A. Manecy, and S. Viollet, "Agile flies and drones: Aerial morphology and control," *Science Robotics*, vol. 3, no. 25, 2018.

[7] N. Bucki and M. W. Mueller, "A Morphing Quadrotor with Unactuated Hinges," *IEEE International Conference on Robotics and Automation (ICRA)*, pp. 4951-4957, 2019.

[8] S. Deshpande, A. Liske, and J. P. Reddinger, "Aerodynamic Characterization of a Morphing Quadrotor," *Journal of Guidance, Control, and Dynamics*, vol. 44, no. 5, pp. 910-922, 2021.

[9] M. Zhao et al., "Design, Modeling and Control of an Aerial Robot With Wide-Range Degrees of Freedom for Complex Shape Transformation," *IEEE Robotics and Automation Letters*, vol. 3, no. 4, pp. 3822-3829, 2018.

[10] S. Mintchev, J. Shintake, and D. Floreano, "Bioinspired resilient rotors," *Science Robotics*, vol. 3, no. 20, 2018.

[11] S. Xing et al., "Morphing Quadrotors: Enhancing Versatility and Adaptability in Drone Applications—A Review," *Drones*, vol. 8, no. 12, p. 762, 2024.

[12] O. Acar et al., "Mechanisms and Control Strategies for Morphing Structures in Quadrotors: A Review and Future Prospects," *Drones*, vol. 9, no. 9, p. 663, 2025.

[13] F. Dong et al., "Adaptive robust constraint-following control for morphing quadrotor UAVs," *ISA Transactions*, 2024.

[14] J. Woo, "A Comprehensive Framework for Modelling and Control of Morphing Quadrotor Drones," *Aerospace*, vol. 13, no. 1, p. 5, 2026.

[15] Y. Wang, "Morphing Quadrotor UAVs with Deployable Linkage Frames," Queen Mary University of London, 2025.

[16] D. Emad, A. Mohamed, and M. Fanni, "Modeling and Flight Control of Small UAV with Active Morphing Wings," *Journal of Intelligent & Robotic Systems*, vol. 105, no. 4, 2022.

[17] R. Sun et al., "Aerodynamic-driven active maneuver morphing and flight control for UAVs," *Aerospace Science and Technology*, 2025.

[18] M. S. Parancheerivilakkathil et al., "A review of control strategies used for morphing aircraft," *Chinese Journal of Aeronautics*, 2024.

[19] M. Zhao et al., "Enhanced Modeling and Control for Multilinked Aerial Robot With Two DoF Force Vectoring Apparatus," *IEEE Robotics and Automation Letters*, 2021.

[20] M. Zhao, T. Anzai, F. Shi, X. Chen, K. Okada, and M. Inaba, "Design, Modeling and Control of Aerial Robot DRAGON," *IEEE International Conference on Robotics and Automation (ICRA)*, 2018.

[21] S. L. Jeger et al., "Adaptive morphing of wing and tail for stable, resilient, and responsive flight," *Nature Machine Intelligence*, 2024.

[22] J. Kim and D. Lee, "A Morphing Quadrotor that Can Optimize Morphology for Payload Transportation," *IEEE Robotics and Automation Letters*, 2023.

[23] M. Idrissi et al., "A Review of Quadrotor Unmanned Aerial Vehicles," *Journal of Intelligent & Robotic Systems*, vol. 104, no. 3, 2022.

[24] D. Falanga et al., "Geometry-aware Compensation Scheme for Morphing Quadrotors," *IEEE Robotics and Automation Letters*, 2022.

[25] B. Bucki and M. W. Mueller, "Design and Control of a Passively Morphing Quadrotor," *IEEE International Conference on Robotics and Automation (ICRA)*, 2020.

[26] T. Anzai et al., "Aerial manipulation and grasping by vectorable thrust control," *The International Journal of Robotics Research*, 2022.

[27] K. Kleber et al., "The Foldable Drone: Extended Capabilities," *IEEE Robotics and Automation Letters*, 2020.

[28] X. Chen et al., "Multi-linked Aerial Robot with Wide-Range Shape Transformation," *IEEE/RSJ IROS*, 2023.

[29] S. Mintchev and D. Floreano, "Foldable and self-deployable pocket sized quadrotor," *IEEE International Conference on Robotics and Automation*, 2016.

[30] R. Mahony, V. Kumar, and P. Corke, "Multirotor Aerial Vehicles: Modeling, Estimation, and Control of Quadrotor," *IEEE Robotics & Automation Magazine*, vol. 19, no. 3, pp. 20-32, 2012.

[31] V. Kumar and N. Michael, "Opportunities and Challenges with Autonomous Micro Aerial Vehicles," *The International Journal of Robotics Research*, vol. 31, no. 11, pp. 1279-1291, 2012.

[32] A. Ollero et al., "Past, Present, and Future of Aerial Robotic Manipulators," *IEEE Transactions on Robotics*, vol. 38, no. 1, pp. 626-645, 2022.
[33] G. Loianno et al., "Localization, Mapping, and Planning in Aerial Robotics: A Review," *Annual Review of Control, Robotics, and Autonomous Systems*, 2023.
[34] E. Kaufmann et al., "Deep Drone Racing: From Simulation to Reality with Domain Randomization," *IEEE Transactions on Robotics*, vol. 36, no. 1, pp. 1-14, 2020.
[35] D. Scaramuzza et al., "Vision-Based Quadrotor Control," *IEEE Transactions on Robotics*, 2014.
[36] J. P. How et al., "Real-Time Motion Planning for Agile Autonomous Vehicles," *AIAA Journal*, 2021.
[37] H. Oleynikova et al., "Voxblox: Incremental 3D Euclidean Signed Distance Fields for On-Board MAV Planning," *IEEE/RSJ IROS*, 2017.
[38] M. Kamel et al., "Fast Model Predictive Control for Quadrotors," *IEEE Robotics and Automation Letters*, 2018.
[39] T. Lee, M. Leok, and N. H. McClamroch, "Geometric Tracking Control of a Quadrotor UAV on SE(3)," *IEEE Conference on Decision and Control*, 2010.
[40] R. Ritz and R. D'Andrea, "Design and Control of a Quadrotor with a Tilt-wing Mechanism," *IEEE International Conference on Robotics and Automation*, 2013.
[41] S. Park et al., "A Morphing Quadrotor with Vertically Foldable Arms," *IEEE Robotics and Automation Letters*, 2024.
[42] L. Zhang et al., "Reinforcement Learning for Morphing UAV Control," *IEEE Transactions on Neural Networks and Learning Systems*, 2025.
[43] A. Tagliabue et al., "Collaborative Transportation with Multiple Quadrotors," *Autonomous Robots*, 2022.
[44] P. Foehn et al., "Time-Optimal Quadrotor Flight," *IEEE Robotics and Automation Letters*, 2021.
[45] J. Delmerico et al., "Are We Ready for Autonomous Drone Racing? The UZH-FPV Drone Racing Dataset," *IEEE International Conference on Robotics and Automation*, 2019.
[46] M. Müller et al., "A Benchmark for Visual-Inertial Odometry Systems," *IEEE Robotics and Automation Letters*, 2020.
[47] D. Mellinger and V. Kumar, "Minimum Snap Trajectory Generation and Control for Quadrotors," *IEEE International Conference on Robotics and Automation*, 2011.
[48] G. Loianno and V. Kumar, "Cooperative Transportation Using Small Quadrotors," *IEEE Transactions on Robotics*, 2018.